International Journal of Heat and Mass Transfer 64 (2013) 783–791

Contents lists available at SciVerse ScienceDirect

International Journal of Heat and Mass Transfer

journal homepage: www.elsevier.com/locate/ijhmt

Vacuum insulation properties of glass wool and opacified fumed silica under variable pressing load and vacuum level

Jongmin Kim, Tae-Ho Song *

School of Mechanical, Aerospace and Systems Engineering, Korea Advanced Institute of Science and Technology, Guseong-dong 373-1, Yuseong-gu, Daejeon, Republic of Korea

ARTICLE INFO

Article history:
Received 27 November 2012
Received in revised form 10 April 2013
Accepted 4 May 2013
Available online 3 June 2013

Keywords:
Vacuum insulation panel
Fumed silica
Glass wool
Thermal conductivity
Pressing load

ABSTRACT

Insulation properties of glass wool (GW) and opacified fumed silica (OFS) as fillers of vacuum insulation panel are experimentally investigated for variable pressing load and vacuum level. Density change of the specimen as a function of the pressing force is measured. The thermal conductivity at center of panel is measured under various vacuum levels and pressing loads. To evaluate the radiative conductivity separately, the diffusion approximation is adopted and the extinction coefficient is measured by an FT-IR apparatus. As the density increases, the solid conductivity increases, while the radiative conductivity decreases to have their sum increased. Pore size is inversely proportional to the density of the material; however, the relation is not consistent in the case of OFS at very low density because of the highly heterogeneous porous structure at that density. Comparing the materials in terms of initial insulation performance at center of panel, we find that GW is superior at low pressing load and the other one is better at high pressing load. Also, OFS turns out to have a longer service-life.

1. Introduction

Energy consumed in building sector takes the greatest portion among the whole energy consumption [1]. Especially, nearly half of the building energy is used for space heating and cooling [2]. This energy is finally dissipated to the environment. Thus, huge amount of energy can be saved if the building insulation is enhanced.

Many countries are trying to regulate insulation of building wall more strictly. In Republic of Korea, for example, the thermal transmittance of building wall is limited to 0.36 $W/m^2 \cdot K$ currently and will be reduced to 0.15 $W/m^2 \cdot K$ by 2017, and 0.08 $W/m^2 \cdot K$ by 2025 [3]. Since any conventional insulator has a thermal conductivity of 0.03–0.04 W/m·K, it needs thickness of more than 40 cm to satisfy the strict regulation. This is nearly impossible, especially for existing buildings which need insulation renovations. For this reason, a superior insulator with much lower thermal conductivity is urgently needed. It will save tremendous amount of energy and at the same time, the valuable building spaces.

As a new insulation method, vacuum insulation panel (VIP) is actively researched recently, as it has very low thermal conductivity (0.002–0.004 W/m K at center of panel) thanks to the evacuated inner space. It is generally composed of an envelope and a core. The envelope helps VIPs to be maintained at a vacuum state. It comprises laminated metal layers on polymer to prevent surrounding gas molecules from penetration. Conduction through the metal layers, in other words, the edge effect is very important issue because high thermal conductivity of them can significantly lower the insulation performance. However it is closely related to the envelope thus not treated in this paper.

Due to the outside atmospheric pressure, VIPs are always pressed. Thus, the core must sustain the pressing force. Insulation performance and service-life of VIPs are heavily dependent on the core material. Porous materials are frequently adopted because they can be evacuated easily. GW and OFS are typical examples in these days [4]. Insulation foams such as polystyrene and polyurethane foam have been used since the early stage thanks to their low price but they have relatively poor insulation performance and large pore size [5]. Phenolic foam may be also employed, but has large pore size, too [6].

Heat transfer in the core takes place by the solid conduction through skeleton of the core, the gas conduction through residual gas, and by the radiation. Each heat transfer mode can be represented by an equivalent conductivity and the total thermal conductivity of the core k_{cop} can be approximated by the sum [7–10];

$$k_{cop} \approx k_g + k_s + k_r, \tag{1}$$

where k_g, k_s and k_r are the gas, solid and radiative conductivities, respectively. The coupling term needs to be considered if water vapor pressure or working temperature is high in OFS-based VIPs [11,12], which effect is not considered in this paper. The gas conductivity is dependent on the gas pressure and can be neglected at a high vacuum. Therefore, the minimum k_{cop}, in other words,

* Corresponding author. Tel.: +82 42 350 3032; fax: +82 42 350 3210.
E-mail address: thsong@kaist.ac.kr (T.-H. Song).

0017-9310/$ - see front matter © 2013 Elsevier Ltd. All rights reserved.
http://dx.doi.org/10.1016/j.ijheatmasstransfer.2013.05.012

Nomenclature

A	area, m^2
e_R	specific Rosseland mean extinction coefficient, m^2/kg
E	extinction coefficient 1/m
H	height of a specimen, m
k	thermal conductivity, W/m·K
l_m	mean free path of a gas molecule, m
P	gas pressure, Pa
P_{ext}	external pressing load, Pa
q	heat transfer rate, W
T	temperature, K

Greek symbols

Π	porosity
ϕ	pore size, m
v	Poisson's ratio
ρ	density, kg/m^3
λ	wavelength, μm
σ	Stefan–Boltzmann constant, $W/m^2 \cdot K^4$
τ	transmittance

Subscripts

cr	critical
cop	center of panel
eff	effective
g	gaseous
r	radiative
R	Rosseland
s	solid

sum of k_s and k_r is achieved at high vacuum. This value is usually the catalog insulation performance of a VIP. Both k_s and k_r strongly depend on the packing density which again depends on the pressing load. If the pressing load is controllable, the insulation performance may be enhanced significantly. Unfortunately, the pressing load on VIPs is fixed at 0.1 MPa as far as the core must withstand the atmospheric pressure. This is true until lately and thus, the initial performance improvement of VIPs has been limited to the suppression of radiation.

Recently, a new type of core is proposed by Kim et al. [13]. It is composed of an artificial structure to support the atmospheric pressure fully or partially, and a separate porous material. Thanks to the artificial structure, the porous material is compressed by 0–0.1 MPa of pressing load. It is anticipated that the insulation performance of this type VIP can be significantly enhanced.

The objective of this paper is to investigate the insulation properties of this new type core under various vacuum levels and pressing loads. GW and OFS are used as the specimen. Heat transfer models to estimate k_{cop} is introduced first and the measurement results using devices such as vacuum guarded hot plate (VGHP) and FT-IR are presented. Finally, characteristics of GW and OFS as the core are discussed in depth.

2. Heat transfer models

The GW sample has a density of 165 kg/m^3 and porosity of 0.92–0.94 when uncompressed. It was made by a Chinese company. The fiber roughly aligned in-plane (Fig. 1(a)) and the fiber diameter is diverse from several hundreds of nanometer to 2 μm (Fig 1(a)). The OFS sample was manufactured by OCI Co., Ltd. It has a density of 45 kg/m^3, porosity of 0.98 when uncompressed and particle diameter of 7–40 nm (Fig 1(b)). It has certain amount of opacifier, whose size and mass fractions are classified. Suffice it to mention that the absorption coefficient is roughly greater than 1 mm^{-1} and this research is intended to reveal the general behavior pattern of OFS.

2.1. Solid conductivity

To predict the solid conductivity, we first review the model of Kwon et al. [14], who derived k_s of fiber and powder by approximating the porous structures. Fiber structure is idealized as beams stacked in staggered manner as shown in Fig. 2. Using this model, the solid conductivity of fiber $k_{s,fiber}$ in the vertical direction can be written as

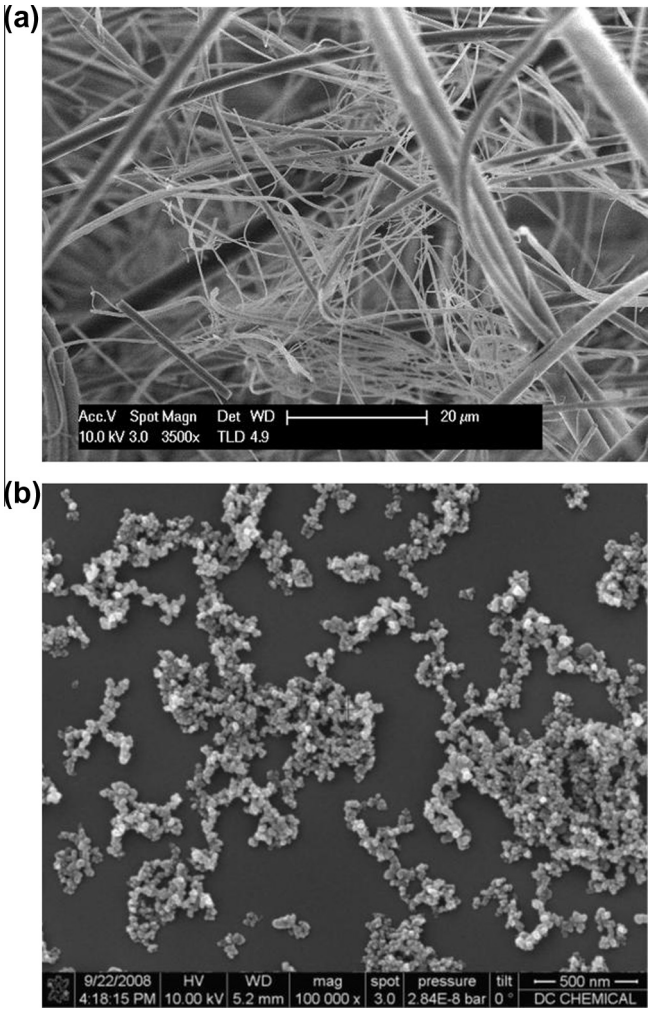

Fig. 1. SEM micrograph of (a) GW and (b) OFS sample (provided from OCI Co. Ltd.).

$$k_{s,fiber}(\theta) = 16k_f \left[\left(\frac{\sqrt{2}\pi^4 E}{48P_{ext}(1-\Pi)^4(1-v^2)} \right)^{1/3} + \frac{\pi^2}{4(1-\Pi)^3 \sin^2\theta} \right]^{-1}, \quad (2)$$

where k_f is the thermal conductivity of fiber at bulk state, P_{ext} is the pressing load, Π is porosity, E and v are the Young's modulus and the Poisson's ratio, respectively and θ is the angle between lay-

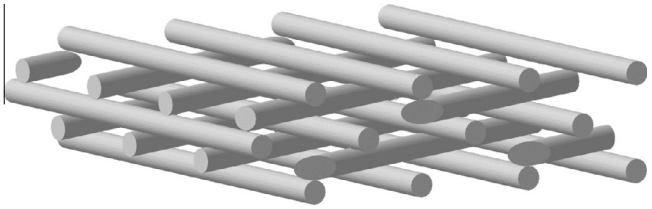

Fig. 2. Idealized structure of GW [14].

ers. Since θ is randomly distributed between 0° and 90°, the arithmetic mean at the solid conductivities over $\Delta\theta$ increments is taken as

$$\overline{k_{s,fiber}(\theta)} = \frac{1}{N}\sum_{i=1}^{N} k_{s,fiber}\left(\frac{i}{N}\Delta\theta\right). \tag{3}$$

Meanwhile, powder is idealized as packed spheres. When spheres are packed vertically in-line, its solid conductivity is expressed as

$$k_{s,powder} = k_p\left(\frac{3(1-\nu^2)P_{ext}}{E}\right)^{1/3}, \tag{4}$$

where k_p is the thermal conductivity of the sphere material.Aside from the theoretical solid conductivities of Eqs. (3) and (4), other empirical relations have been widely used. For fiber materials, Kamiuto et al. [15] express the solid conductivity with porosity Π of the material as

$$k_{s,fiber} = (1-\Pi^{2/3})fk_f, \tag{5}$$

where f is a correction factor which is determined experimentally. Since f accounts for the shape, length, area of heat conduction path, it is actually a function of Π. Wang et al. [16] suggest a simple relation as

$$k_{s,fiber} = A + (B\cdot\rho)k_f, \tag{6}$$

where A and B are constants to be found. Powder has empirical relations which are similar to those of fiber. Hummer et al. [8] express $k_{s,powder}$ as

$$k_{s,powder} = k_p(1-\Pi)^{1.5}, \tag{7}$$

which Caps and Fricke [9] has derived a relation between $k_{s,powder}$ and P_{ext} for several kinds of powder materials;

$$k_{s,powder} = C(P_{ext})^D. \tag{8}$$

Constants C and β are experimental constants. As an example, perlite shows $C = 5$ and $D = 0.37$ and precipitated silica shows C and D of 1.8 and 0.56, respectively [9].

2.2. Gas conductivity

The mean free path l_m of air in a continuum state can be expressed as [17]

$$l_m = \frac{2.19\times10^{-5}T}{P}, \tag{9}$$

where T is temperature in K and P is the gas pressure in Pa. If the pressure is sufficiently small so that the mean free path is larger than the pore size, gas conduction mechanism is totally changed from the Fourier's law. Smoluchowski expresses heat flux by rarefied gas conduction as [18]

$$k_g = \frac{k_{g0}}{\phi+2\beta}\phi, \tag{10}$$

where k_{g0} is the continuum thermal conductivity, ϕ is the pore size of porous material in m and β is a function of the constant pressure to constant volume specific heat ratio. For air, β can be expressed as

$$\beta = \left(5.35\times10^{-5}\right)\frac{T}{P}. \tag{11}$$

The gas conductivity k_g is derived by combining Eqs. (10) and (11) as

$$k_g = \frac{k_{g0}}{1+\frac{(1.07\times10^{-4})T}{\phi P}}. \tag{12}$$

For air at room temperature, $k_{g0} \approx 0.026$ W/m·K.

2.3. Radiative conductivity

VIP core materials usually have large optical thicknesses. The optical thickness is defined as the product of the extinction coefficient and the material thickness. If it is much larger than unity, radiative heat transfer through the material can be approximated by a conduction equation as [19–21]

$$q_r = -\frac{16\sigma T^3}{3E_R}\frac{dT}{dz}, \tag{13}$$

here σ is the Stefan–Boltzmann constant, E_R is the Rosseland mean extinction coefficient (the specific Rosseland mean extinction coefficient e_R times density ρ). The Rosseland mean extinction coefficient is expressed by an integral of the spectral extinction coefficient E_λ as

$$\frac{1}{E_R} = \frac{C_1C_2}{4\sigma T^5}\int_0^\infty \frac{1}{E_\lambda}\cdot\frac{1}{\lambda^6}\left[\exp\left(\frac{C_2}{\lambda T}\right)-1\right]^{-1}d\lambda, \tag{14}$$

where $C_1 = 3.74$ W·m^2 and $C_2 = 0.014388$ m·K. If the spectral transmittance τ_λ is given, E_λ can be found from following relation.

$$E_\lambda = -\ln(\tau_\lambda)/H, \tag{15}$$

where H is the specimen thickness. Spectral transmittance τ_λ is measured in this research using a commercial FT-IR device (IFS 66/s from Bruker corp.) with 2.5–20 μm of wavelength range. OFS sample is measured by KBr method. Very small amount of OFS powder is mixed with pulverized KBr and formed into a pellet by pressing. The thickness of OFS + KBr pellet is 0.15 mm. Since E_R from the FT-IR measurement is valid only for the density of OFS in the pellet, it is divided by the density to find e_R. As the results, e_R of GW and OFS samples are measured as 52 m^2/kg and 90 m^2/kg, respectively at 298 K. For comparison, e_R of non-opacified fumed silica is measured to be 23 m^2/kg.

3. Experiments

3.1. Measurement of density at various pressing loads

Both GW and OFS are highly porous and soft. They are easily deformed when pressing load is exerted. As shown in Section 2.1, k_s changes under different pressing loads. Density or porosity change can be derived by measuring the thickness change of the samples. It is measured by an apparatus developed by the authors as shown in Fig. 3. It is composed of an air-cylinder, a linear variable differential transformer (LVDT) sensor, and a load cell. The air-cylinder is operated using compressed air and a regulator. The upper plate is connected to the air-cylinder to press the specimen. The bottom plate is placed on a load cell and it is free to move. Thus the pressing force is measured by the load cell when the specimen is pressed by the upper plate. The LVDT sensor measures the displacement of the upper plate which is indeed the thickness change of the specimen. Structurally, the upper and bottom plates are parallel to each other.

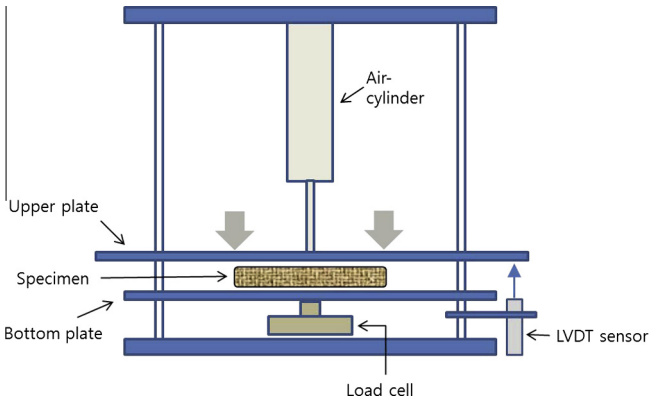

Fig. 3. Measurement apparatus for thickness change with pressing load.

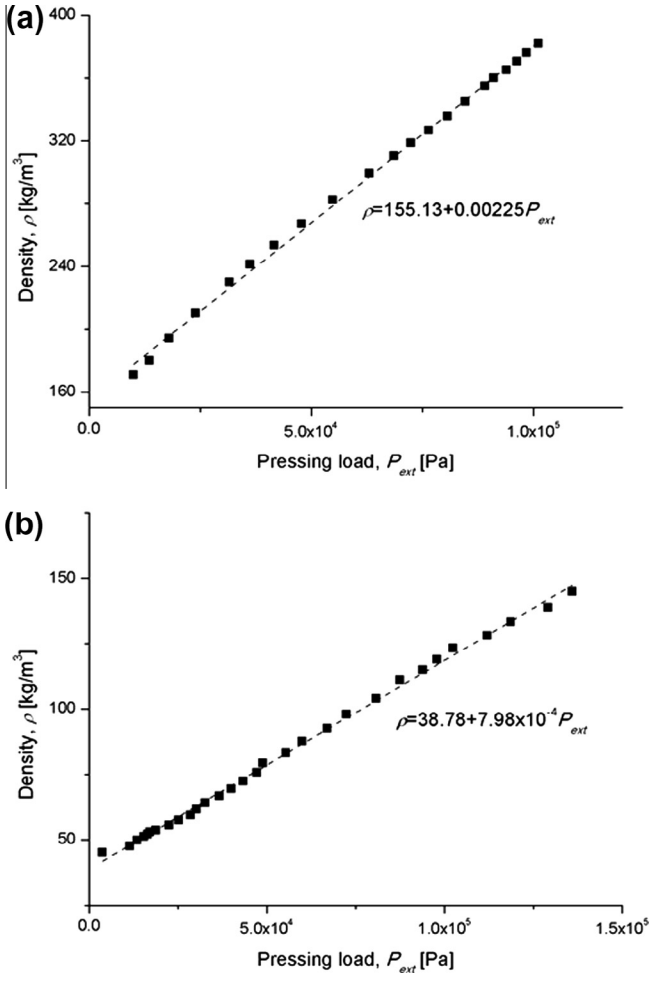

Fig. 4. Density change of (a) GW and (b) OFS.

Fig. 4 shows density change of the specimen. Densities of both specimen increase linearly as the pressing load increases. The GW density (kg/m^3) is fitted as

$$\rho = 155.13 + 2.25 \times 10^{-3} P_{ext} \tag{16}$$

with 0.9% relative error and for OFS,

$$\rho = 38.78 + 7.98 \times 10^{-4} P_{ext} \tag{17}$$

with 1.5% relative error, respectively. Here, P_{ext} is the pressing load in Pa. When the pressing load is released, GW returns back to the original thickness but OFS is plastically deformed and remains at the pressed thickness.

3.2. Measurement of the thermal conductivity

3.2.1. Measurement apparatus

There are several measurement methods for the thermal conductivity such as laser flash, heat flow meter, guarded hot plate method, and etc. For VIPs, the guarded hot plate (GHP) method is known to be the most precise method [22]. To make measurements under various vacuum levels and pressing loads, a measurement apparatus, called vacuum guarded hot plate (VGHP) apparatus, is fabricated by the authors. Three different parts comprise the VGHP apparatus, each performing different functions (see Fig. 5).

The thermal conductivity is measured by the GHP part. The heater block, which is controlled by an electric heater and a power supply, is placed at the center. It is made of pure copper and has a dimension of $150 \times 150 \times 50$ mm^3. Sides of the heater block are covered by a guard-ring across a narrow gap. The guard-ring has an inner water channel and it is connected to a bath circulator. Its outer dimension is $300 \times 300 \times 50$ mm^3. The hot plate is placed beneath the heater block/guard-ring unit. It also has a dimension of $300 \times 300 \times 50$ mm^3 and its temperature is controlled by the same way as the guard-ring. A specimen is sandwiched between the heater block/guard-ring unit and the cold plate. The cold plate is identical to the hot plate but maintained cold as a heat sink.

Generated heat from the heater block is totally transferred to the cold plate via the specimen when temperatures of the guard-ring and the hot plate are same as that of the heater block. The thermal conductivity of the specimen is then calculated as

$$k_{meas} = \frac{q_{heater} h}{A_{heater} \Delta T}, \tag{18}$$

where q_{heater} is the heat generation rate from the heater block, h is thickness of specimen, A_{heater} is a surface area of the heater block, and ΔT is the temperature difference between upper and bottom surfaces of the specimen.

The GHP part is installed in a vacuum chamber. The chamber is evacuated by a diffusion pump to approximately 10^{-4} Pa. External pressing load is exerted by the pressure pad (Fig. 5). It is actually an air cylinder. When the pressure of inner space rises, the moving part moves up and presses the specimen. Here, a rigid dummy is inserted between the cold plate and the upper wall of the vacuum chamber to counter-support the pressing load.

3.2.2. Measurement condition and specimen

Thermal conductivities of two samples are measured under different vacuum levels and external pressing loads. The mean temperature of the sample is maintained at 298 K (heater block at 308 K and cold plate at 288 K). When the chamber is evacuated, the pressing load cannot be below 0.1 MPa unless the pressure pad is evacuated. For this reason, the pressing load below 0.1 MPa is controlled indirectly by changing the specimen thickness. In Fig. 6, the GW sample has an original thickness H_0. If dummy pillars of height H are inserted between the GHP components, the sample is pressed to thickness H and excessive pressing force is supported by the pillars. The pure pressing load on the specimen can be easily found from Eq. (16).

Unlikely GW, OFS particles are so fine that they cannot be contained in the measurement apparatus in the same way as before. Thus, it is contained in a housing made by polycarbonate as shown in Fig. 7. Thickness of the sample is at first H_0 and is pressed to $H_0 - H_c$ with a cap of thickness H_c. Exerted pressing load on the sample can be found using Eq. (17). Thickness (or density) as well as pressing load can be adjusted by changing H_c.

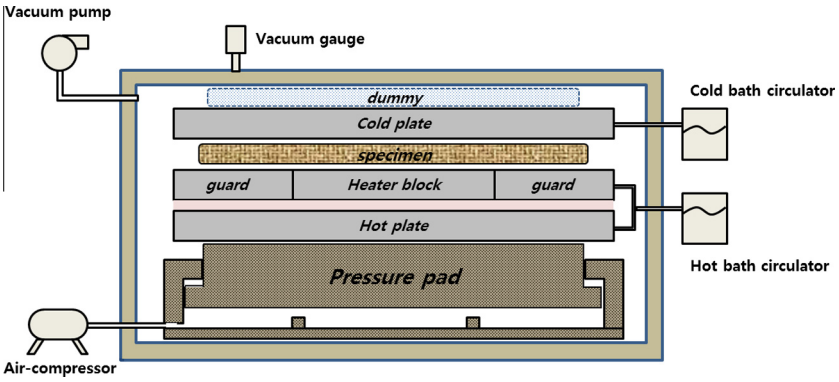

Fig. 5. Schematic composition of VGHP apparatus.

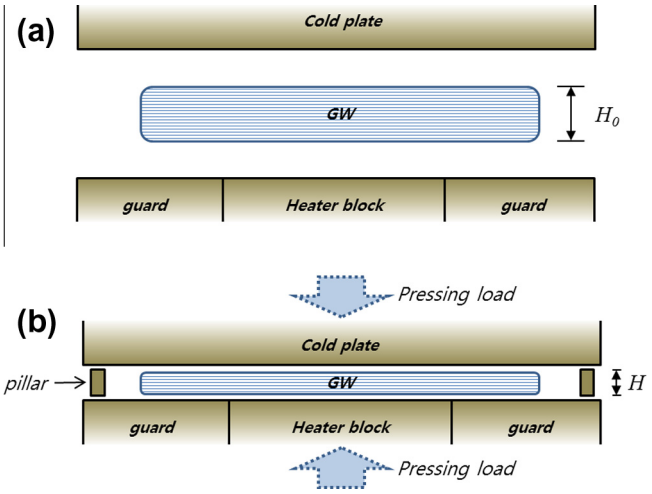

Fig. 6. GW sample (a) before and (b) after pressing in the VGHP.

Height H in GW and H_0 in OFS measurement must not change when pressing force is exerted. Thus they are checked before and after measurements using height gauge (192 HDM-30A by CAS MIS co.LTD) which has uncertainty of ±20 μm.

3.2.3. Uncertainty analysis of the measurement

From Eq. (18), the uncertainty of measured k_{meas} can be estimated as [23]

$$\frac{dk_{meas}}{k_{meas}} = \sqrt{\left(\frac{\partial k_{meas}}{\partial A_{heater}}\frac{dA_{heater}}{k_{meas}}\right)^2 + \left(\frac{\partial k_{meas}}{\partial(\Delta T)}\frac{d(\Delta T)}{k_{meas}}\right)^2 + \left(\frac{\partial k_{meas}}{\partial h}\frac{dh}{k_{meas}}\right)^2 + \left(\frac{\partial k_{meas}}{\partial q_{heater}}\frac{dq_{heater}}{k_{meas}}\right)^2}. \quad (19)$$

Uncertainties from A_{heater}, ΔT and h are only 0.03%, 0.4% and 0.2%, respectively. The major uncertainty comes from q_{heater}, which has uncertainties of voltage and current of the power supply device. It increases as q_{heater} decreases; smaller k_{meas} means larger uncertainty. When k_{meas} is around 1 mW/m·K, the uncertainty of q_{heater} is approximately 8%, resulting in k_{meas} slightly larger than 8%.

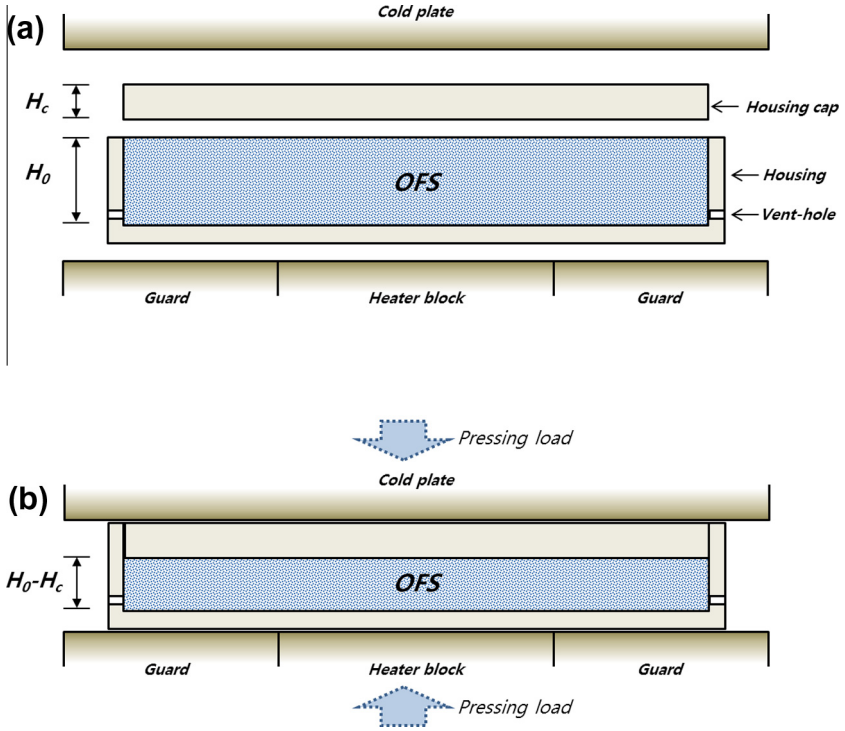

Fig. 7. OFS sample (a) before and (b) after pressing in the VGHP.

4. Results and discussions

4.1. Glass wool (GW)

Fig. 8(a) shows k_{cop} of the GW sample at different vacuum pressures and sample densities. As the pressure decreases, k_{cop} drops rapidly because k_g decreases. When k_g is virtually zero (when $P \leqslant 1Pa$), k_{cop} stays constantly from 1.2 to 3.4 mW/m·K, with the variation depending on the sample densities. The radiative conductivity k_r can be estimated by the method of Section 2.3. Hence, k_s can be found by subtracting k_r from k_{cop}. When the GW density increases, it is difficult for the photons to penetrate through the sample thus the extinction coefficient E_R increases and k_r decreases. At the same time, the contact area and the number of contact points between fibers increase thus k_s increases. As the result, the sum of k_s and k_r increases with density (Fig. 9(a)). Fricke et al. [24] and Kamiuto et al. [15] also report similar relation between k_{cop} and ρ.

On the other hand, Wang et al. [16] report a different relation. They observed that k_{cop} decreases as ρ increases in a low range of ρ. However, when extrapolating k_{cop} at high ρ range using the empirical relation of Wang et al., k_{cop} increases again (see Fig. 10). This phenomenon can be explained by the relative portions of k_r and k_s; k_r dominates at low ρ range to make k_{cop} inversely proportional to ρ, but k_s dominates at high ρ range to make the opposite trend. From this discussion, we can say that there is an optimum density that the sum of k_r and k_s is minimized at a given temperature. The radiative conductivity k_r is proportional to third power of temperature thus the optimum density will increase at higher temperature.

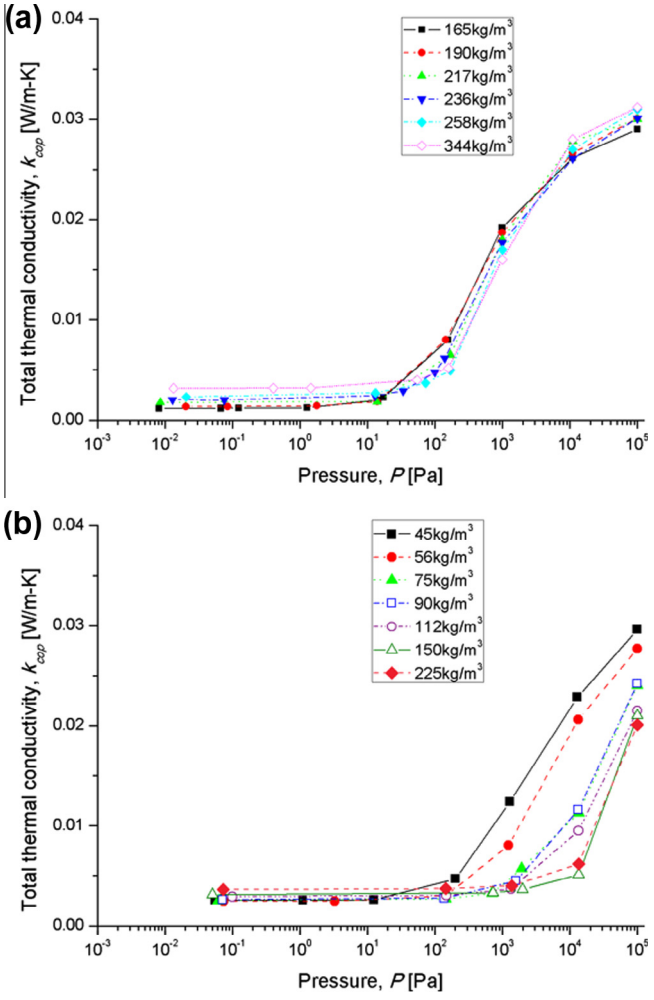

Fig. 8. Total thermal conductivities of (a) GW and (b) OFS at various vacuum levels and densities.

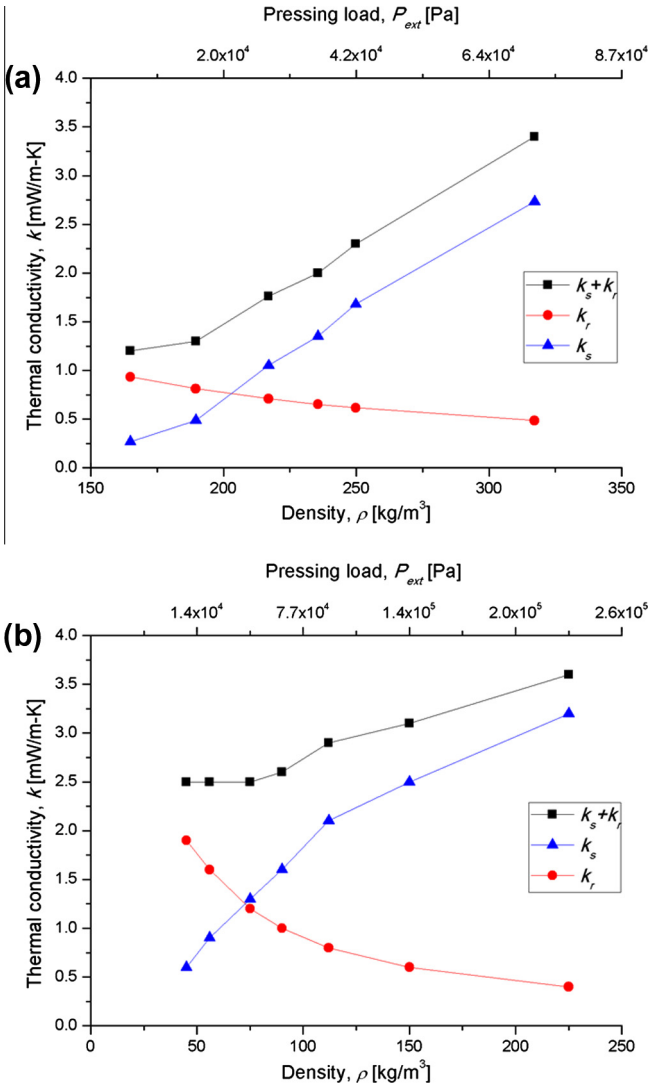

Fig. 9. Sum of k_s and k_r of (a) GW and (b) OFS with different sample densities at high vacuum (pressing load is plotted from Fig. 4).

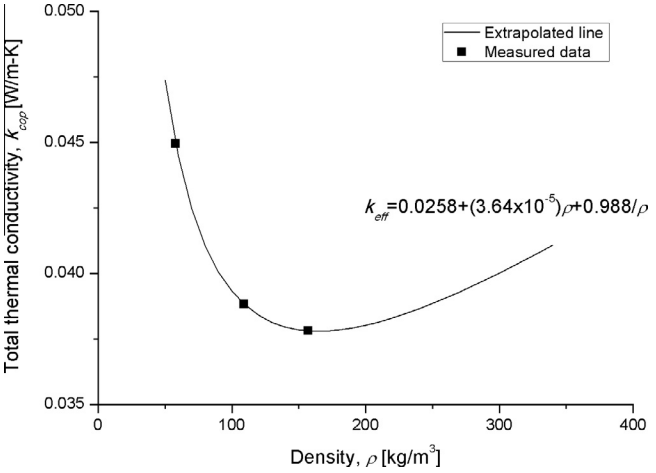

Fig. 10. Measured k_{cop} of GW with ρ (dots) and extrapolated curve from the literature [16].

Besides of the optimal density, k_r can be decreased by inserting radiation shields between glass wool sheets. Radiation shield is a metal-coated polymer film with an emissivity as low as those of aluminum, silver, and etc. The radiative conductivity is usually inversely proportional to number of radiation shields. Therefore inserting as many shields as possible would be good if glass wool sheet is thin enough. The only worry is that the metal and polymer layers may increase the solid conduction in spite of its very small thickness. Therefore, the merits and demerits and the optimal number of radiation shields need to be studied for a practical application.

As explained in Section 2.1, the solid conductivity can be estimated using the theoretical relations (Eqs. (2) and (3)) or empirical ones (Eqs. (5) and (6)). As compared in Fig. 11, theoretical relation by Eqs. (2) and (3) shows larger k_s then the measured one. The reason of this discrepancy is that the porous structure used in the theoretical model (Fig. 2) is assuming uniform contact between fibers, which is quite different from the actual structure of GW (Fig. 1(a)). Also, the theoretical model only accounts for the change of the contact area according to the variation of P_{ext} but changing number of contact points is not considered. Thus it is recommended to use the empirical relation when estimating k_s as a function of density (or porosity/pressing load) of GW. Further refinement of the theoretical model is also called for.

4.2. Opacified fumed silica (OFS)

Measured k_{cop} of OFS was also shown in Fig. 8(b). It shows similar behavior as GW. At low pressure ($P \leqslant 10$Pa), k_{cop} is around 2.5–3.6 mW/m·K. The radiative conductivity and the solid conductivity are separated using the FT-IR measurement of Section 2.3 and are plotted in Fig. 9(b). The relation between the thermal conductivity and the density is similar to that of GW. The solid conductivity of this sample (Fig. 12) is very close with 5% relative error to that of precipitated silica measured by Caps and Fricke [9] at various pressing load, with 15% relative error to that of fumed silica measured by Quenard and Sallee [25] and Caps et al. [26]. The radiative conductivity at low density is still large despite the existence of the opacifier (see Fig. 9).

In fact, opacifier is essentially needed at low density because it greatly increases e_R of the fumed silica from 23 m^2/kg to 90 m^2/kg as shown in Section 2.3. On the other hand, using opacifier at high density has to be considered carefully because k_r is already small so that the effect of the opacifier is not significant while k_s may be increased; opacifiers usually have higher thermal conductivity than powder insulator. Therefore, they are believed to increase the solid conduction of the mixture. Note that, however, the opposite effect can also be found [9,27]. Density of the mixture seems to affect k_s more than the amount of the opacifier does.

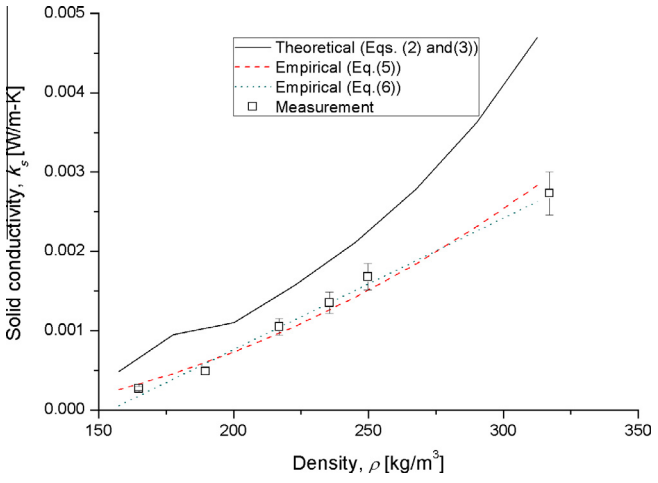

Fig. 11. Comparison between theoretical/empirical relations of the glass wool k_s with the measurement (error bars: ±10%).

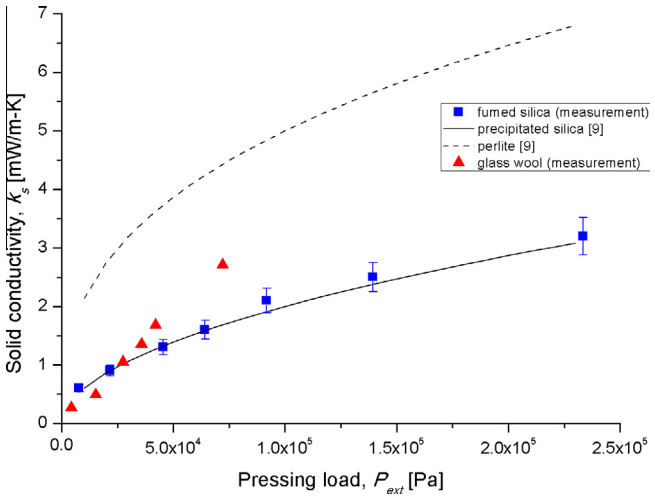

Fig. 12. Solid conductivities of several materials (error bars: ±10%).

Theoretically estimated k_s from Eq. (4) using parameters $k_p = 1.3$ W/m·K, $E = 73$ GPa and $\nu = 0.17$ shows much larger value than the measurement (for example, when $P_{ext} = 0.1$ MPa, k_s by Eq. (4) is 21 mW/m·K but the measurement is about 2 mW/m·K). It is reasoned that the theoretical model assumes an unrealistic orderly vertical stacking of identical spheres. Thus, more realistic modeling should be made. For now, when estimating k_s of OFS or other powder insulator, using an empirical relation is recommendable rather than the theoretical relation.

As explained in Section 2.2, pore size of the core material heavily affects the gas conduction. In a strict sense, various pore sizes are distributed in the core material. Using an effective pore size is desirable in the real application. The determination method of Lee et al. [28] is an appropriate method in that regard; They retro-fitted ϕ using Eq. (12) from measured k_g. Table 1 shows the effective pore sizes for various densities of GW and OFS. Pore sizes of GW are much larger than those of OFS. Increasing density means decreasing thickness of the core material therefore, pore size and density show inversely proportional relations.

Ideally, if the density increases, for example by two times, pore size should decrease to half. The measured densities of GW and highly packed OFS satisfy such relations. However, pore sizes at low-density OFS (cases of 45 and 56 kg/m^3) are much larger than

Table 1
Effective pore size for various densities of GW and OFS using Eq. (12).

Sample	Density, ρ [kg/m^3]	Pore size, ϕ [μm]
GW	165	75
	190	61
	217	48
	235	42
	258	31
	344	26
OFS	45	12.8
	56	6.96
	75	1.60
	90	1.44
	113	0.80
	150	0.55
	225	0.36

expected. The reason of this discrepancy can be roughly estimated from the microphotograph of OFS.

Fig. 13(a) shows the surface of unpressed one; it is highly uneven. In the figure, nano-sized particles congregate with each other and form agglomerates One sees mixture inhomogeneity with sizes of 1–2 mm. Gaps of 0.5–2 mm are also observed. On the contrary, if it is pressed as shown in Fig. 14(a), large gaps are not observed any more. Cross section of unpressed case (Fig. 13(b)) still has large voids sized in several hundred micron but that of pressed case (Fig. 14(b)) has very fine and even aggregates. From this observation, we may reason that the pore size is very uneven at the low-density OFS and such unevenness makes it depart from the regular relation between the pore size and the density.

Due to the fine aggregate sizes, fumed silica or other powder insulators are not easy to handle. They are generally packed with high pressing load when used in the VIPs. For this reason, studies about those materials usually have dealt with high densities over 100 kg/m^3. However, as shown above, OFS at low density has better insulation performance, though uneven porous structure at very low density may bring additional effects. Thus, insulation properties at low density and uneven porous structure need to be studied further to find potential merits for the VIP applications.

4.3. Vacuum insulation characteristics

Regarding the core material of VIPs, two major properties are usually considered: the insulation performance and service-life. Initial thermal conductivity at the center of VIPs is the sum of k_s and k_r. When comparing the solid conductivities of the two samples under study, GW shows slightly lower k_s for light pressing load ($P_{ext} \leqslant 25$ kPa) but becomes higher as P_{ext} increases (Fig 12). When $k_r + k_s$ are compared (Fig. 9), difference between these two samples becomes larger than k_s alone. In a word, GW has better insulation performance at $P_{ext} \leqslant 25$ kPa but OFS is superior at higher pressing force. GW has been known to have better insulation performance than OFS at low vacuum pressure [11] but an exceptional case can be found as shown here.

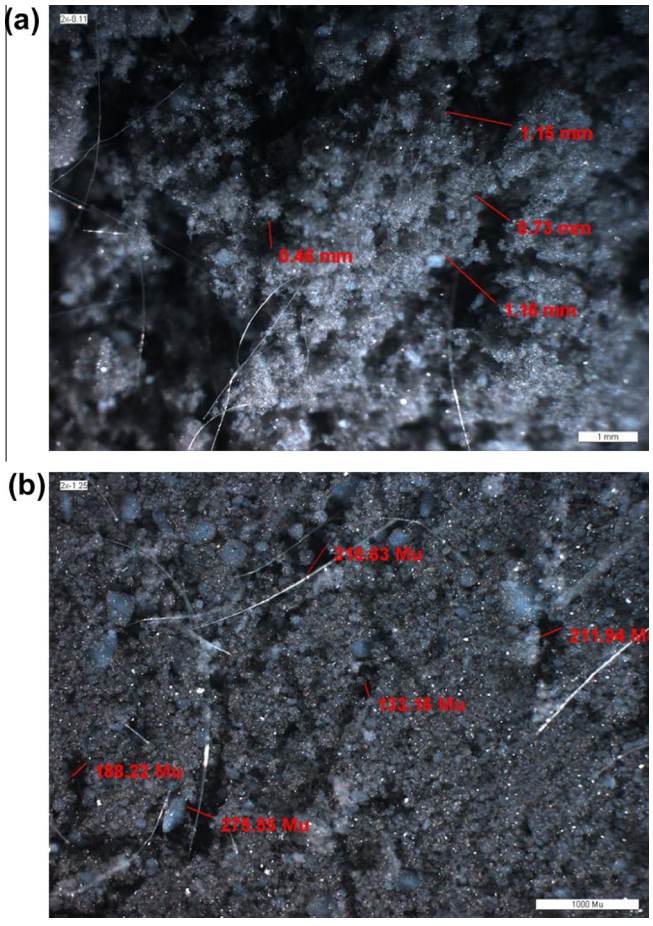

Fig. 13. Microphotograph of OFS at very low density; (a) surface, unpressed (b) cross section, unpressed.

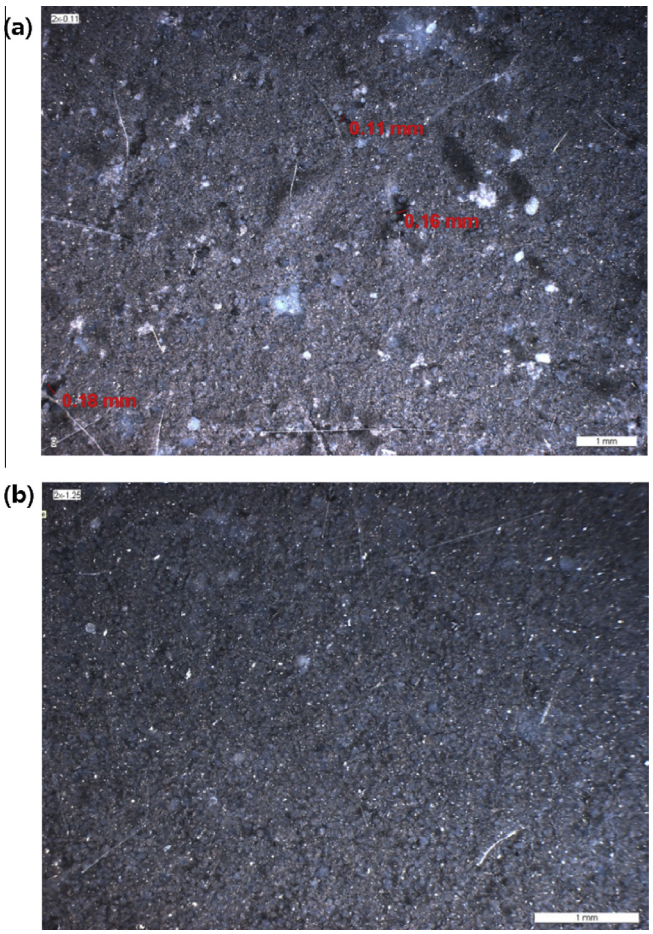

Fig. 14. Microphotograph of OFS at moderate density; (a) surface, pressed (b) cross section, pressed.

Though a VIP is sealed in an envelope, inner pressure rises up with time. As measured with the vacuum level, k_{cop} also rises with the pressure (see Fig. 8). If k_{cop} rises above a critical value, it cannot function as a VIP any more. Therefore, to extend the service-life of VIPs, the rate of vacuum pressure rise should be minimized or the effective pore size of the core has to be as small as possible (see Eq. (12)). The former is heavily dependent on the permeation characteristics of the envelope thus it is not treated here. When comparing the pore size, GW has much larger average pore size than the other one. If the critical pressure P_{cr} is defined as the pressure at which

$$k_{cop} = \frac{1}{2}\left(k_{cop,\max} + k_{cop,\min}\right), \tag{20}$$

where $k_{cop,max}$ is the maximum k_{cop}, that is, k_{cop} at the atmospheric pressure and $k_{cop,min}$ is the minimum k_{cop}, that is, $k_s + k_r$. Then, GW and OFS compressed at P_{ext} = 1 atm have P_{cr} of approximately 1 kPa and 20 kPa, respectively.Once P_{cr} is determined, service-life can be roughly estimated from the knowledge of the inner void volume

and vacuum pressure increase rate [29]. Imagine that the core has a dimension of $30 \times 30 \times 1$ cm. Assume that inner void volume and vacuum pressure increase rate are 720 cm^3 and 2×10^{-6} Pa L/s, respectively. Then, service-life of GW VIP is 11 years and that of OFS VIP is 230 years. Notice that above estimation is a simplified one. Other aging factors, especially mass transfer of water vapor has to be considered [11,12] for an accurate estimation.As a final remark, to realize the actual VIPs with artificial structure, cover plates and pillars are needed to control the pressing load on the core. Then, the heat transfer through the core may be decreased but artificial structure brings about additional heat transfer. Parallel studies are under way to find the optimized artificial structure and the cover plates.

5. Conclusion

Vacuum insulation properties of GW and OFS are investigated using theoretical models and experiments. Relation between density and external pressing load is measured first and radiative properties are measured using an FT-IR device. The VGHP device is developed for the measurement of k_{cop} at different vacuum level and pressing load. As the result, k_s and k_r are found at different density and the effective pore sizes are derived. To estimate k_s, using the empirical relation is found to be more accurate and practical for both materials. As the density increases, k_s increases but k_r decreases to make an optimum density at which $k_s + k_r$ is minimized. The effective pore sizes are inversely proportional to the density but the relation is not consistent at low density of OFS because of uneven porous structure at that density. GW is superior in terms of the center of panel insulation performance when the pressing load is less than 25 kPa but OFS is better when it is larger. In terms of the service-life of VIPs, OFS has much longer one thanks to the smaller average pore size.

Acknowledgments

This paper was supported by the National Research Foundation of Korea (NRF) grant funded by the Korea Government (MEST) (No. 2012-047641) and the second stage of the Brain Korea 21 Project in 2012. The authors thank OCI Co. for the offer of their fumed silica sample.

References

[1] Nature Publishing Group, Architects of a low-energy future, Nature 452 (2008) 520–523.
[2] 2010 Buildings Energy Data Book, U.S. Department of Energy, 2011.
[3] Ministry of Land, Transport and Maritime Affairs of R. Korea, Vitalize plan for green city and building, 2009.
[4] P. Mukhopadhyaya, K. Kumaran, N. Normandin, D. Reenen, J. Lackey, High-performance vacuum insulation panel: development of alternative core materials, ASCE J. Cold Reg. Eng. 22 (2008) 103–123.
[5] J. Ficke, U. Heinemann, H.P. Ebert, Vacuum insulation panels-from research to market, Vacuum 82 (2008) 680–690.
[6] J. Kim, J.H. Lee, T.H. Song, Vacuum insulation properties of phenolic foam, J. Heat Mass Transfer 55 (2012) 5343–5349.
[7] J. Fricke, X. Lu, P. Wang, D. Buttner, U. Heinemann, Optimization of monolithic silica aerogel insulants, J. Heat Mass Transfer 35 (1992) 2305–2309.
[8] E. Hummer, Th. Rettelbach, X. Lu, J. Fricke, Opacified silica aerogel powder insulation, Thermochim. Acta 218 (1993) 269–276.
[9] R. Caps, J. Fricke, Thermal conductivity of opacified powder filler materials for vacuum insulations, Int. J. Thermophys. 21 (2000) 445–452.
[10] E. Hummer, X. Lu, Th. Rettelbach, J. Fricke, Heat transfer in opacified aerogel powders, J. Non-Cryst. Sol. 145 (1992) 211–216.
[11] J. Fricke, H. Schwab, U. Heinemann, Vacuum insulation panels-exciting thermal properties and most challenging applications, Int. J. Thermophys. 27 (2006) 1123–1139.
[12] M. Bouquerel, T. Duforestel, D. Baillis, G. Rusaouen, Heat transfer modeling in vauum insulation panels containing nanoporous silicas–a review, Energy Build. 54 (2012) 320–336.
[13] J. Kim, T.H. Song, I. Yeo, B.S. Choi, The 2nd Generation Vacuum Insulation Panel, International Conference on Applied Energy, Suzhou, China, 2012.
[14] J.S. Kwon, C.H. Jang, H. Jung, T.H. Song, Effective thermal conductivity of various filling materials for vacuum insulation panels, J. Heat Mass Transfer 52 (2009) 5525–5532.
[15] K. Kamiuto, I. Kinoshita, Y. Miyoshi, S. Hasegawa, Experimental study of simultaneous conductive and radiative heat transfer in ceramic fiber insulation, J. Nucl. Sci. Technol. 19 (1982) 460–468.
[16] H. Wang, R.B. Dinwiddie, K.E. Wilkes, T. Huff, G-Plus Report to Owens Corning Thermal Conductivity Measurements of Fiberglass, Oak Ridge National Laboratory and Owens Corning Inc., 2003.
[17] A. Roth, Vacuum Technology, 3rd ed., Elsevier, New York, 1990. pp. 37–44.
[18] J.M. Lafferty, Foundations of Vacuum Science and Technology, John Willey & Sons, New York, 1998. 50–51.
[19] S.Y. Zhao, B.M. Zhang, X.D. He, Temperature and pressure dependent effective thermal conductivity of fibrous insulation, Int. J. Therm. Sci. 48 (2009) 440–448.
[20] K. Daryabeigi, G.R. Cunnington, J.R. Knutson, Combined heat transfer in high-porosity high-temperature fibrous insulation: theory and experimental validation, J. Thermophys. Heat Transfer 25 (2011) 536–546.
[21] C.J. Tseng, K.T. Kuo, Thermal radiative properties of phenolic foam insulation, JQSRT 72 (2002) 349–359.
[22] R.E. Collins, C.A. Davis, C.J. Dey, S.J. Robinson, J.Z. Tang, G.M. Turner, Measurement of local heat flow in flat evacuated glazing, J. Heat Mass Transfer 36 (1993) 2553–2563.
[23] J.P. Holman, Experimental Methods for Engineers, 6th ed., McGraw-Hill, 1994.
[24] J. Fricke, D. Buttner, R. Caps, J. Gross, O. Nilsson, Solid conductivity of loaded fibrous insultaions, in: D.L. McElroy, J.F. Kimpflen (Eds.), Insulation Materials, Testing, and Applications, ASTM STP 1030, American Society for Testing and Materials, Philadelphia, 1990, pp. 66–78.
[25] D. Quenard, H. Sallee, Micro-nano porous materials for high performance thermal insulation, in: Proceedings of the 2nd International Symposium on Nanotechnology in Construction, Bilbao, Spain, 2005.
[26] R. Caps, U. Heinemann, M. Ehrmanntraut, J. Fricke, Evacuated insulation panels filled with pyrogenic silica powders: properties and applications, High Temp. High Press. 33 (2001) 151–156.
[27] Th. Rettelbach, J. Sauberlich, S. Korder, J. Fricke, Thermal conductivity of silica aerogel powders at temperatures from 10 to 275K, J. Non-Cryst. Sol. 186 (1995) 278–284.
[28] O.J. Lee, K.H. Lee, T.J. Yim, S.Y. Kim, K.P. Yoo, Determination of mesopore size of aerogels from thermal conductivity measurements, J. Non-Cryst. Sol. 298 (2002) 287–292.
[29] J.S. Kwon, C.H. Jang, H. Jung, T.H. Song, Vacuum maintenance in vacuum insulation panels exemplified with a staggered beam VIP, Energy Build. 42 (2010) 590–597.